Finite-Difference Outer-Layer, Analytic Inner-Layer Method for Turbulent Boundary Layers

Richard A. Wahls*
North Carolina State University, Raleigh, North Carolina
Richard W. Barnwell†
NASA Langley Research Center, Hampton, Virginia
and
Fred R. DeJarnette‡
North Carolina State University, Raleigh, North Carolina

A new turbulent boundary-layer method is developed which models the inner region with the law of the wall, whereas the outer region uses Clauser's eddy viscosity in Matsuno's finite-difference method. The match point between the inner and outer regions, as well as the wall shear stress, is determined at each marching step during the computation. Results obtained for incompressible, two-dimensional flow over flat plates and ellipses are compared with solutions from a baseline method that uses a finite-difference method for the entire boundary layer. Since the present method used the finite-difference method in the outer region only, the number of grid points required was about half that needed for the baseline method. Accurate displacement and momentum thicknesses were predicted for all cases. Skin friction was predicted well for the flat plate, but the accuracy decreased significantly for the ellipses. Adding a wake function to the law of the wall allows some of the pressure gradient effect to be taken into account, thereby increasing the accuracy of the method.

Nomenclature

a_j = coefficient vector in Eq. (13b)
A = van Driest damping factor defined in Eq. (6), m
A_j = coefficient vector in Eq. (13b)
b = ratio of total viscosity to molecular viscosity
B = empirical constant in the log law of the wall
BA = ratio of semiminor to semimajor axes of an ellipse
B_j = coefficient vector in Eq. (13b)
c_j = coefficient vector in Eq. (13a)
C_j = coefficient vector in Eq. (13b)
CF = skin-friction parameter $C_f Re_x^{1/2}$
C_f = local skin-friction coefficient $2\tau_w/\rho U_e^2$
C_1-C_3 = coefficients given in Eq. (27)
D_j = coefficient vector in Eq. (13b)
DEN = matrix solver parameter, defined by Eq. (A3)
e_j = coefficient vector, defined by Eq. (A2)
E_j = coefficient vector, defined by Eq. (A2)
f = stream function parameter $\int F d\eta$
F = velocity ratio u/U_e
G_j = coefficient vector, defined by Eq. (A2)
H = shape factor δ^*/θ
J_{max} = number of grid points across the entire boundary layer
J_{req} = number of points across the boundary layer required for the finite-difference solution
K = Clauser's empirical constant, 0.0168
L = reference length, m
Re = freestream Reynolds number $U_\infty L/\nu$
Re_x = local Reynolds number $U_e x/\nu$
u,v = x and y (or η) velocity components, m/s
u^* = friction velocity, m/s
u^+ = inner variable velocity
U_e = velocity at the edge of the boundary layer, m/s
$\bar{U}_e$ = U_e/U_∞
U_∞ = freestream velocity, m/s
WF = White's linear wake function, defined by Eq. (30)
x = surface coordinate, m
$\bar{x}$ = x/L
y = coordinate normal to the surface, m
y^+ = inner variable coordinate normal to the surface
α = wake function parameter, defined by Eq. (30)
β = inviscid function of x, defined by Eq. (9)
δ^* = displacement thickness, m
η = transformed coordinate normal to the surface, defined by Eq. (9)
θ = momentum thickness, m
κ = von Kármán constant
ν,ν_T = kinematic laminar and turbulent viscosities, m^2/s
ρ = density, kg/m^3
τ = shear stress, N/m^2
ϕ = angular coordinate

Subscripts

i = inner region
i,j = indices of the grid point system
m = match point
o = outer region
w = wall

Presented as Paper 87-0429 at the AIAA 25th Aerospace Sciences Conference, Reno, NV, Jan. 12-15, 1987; received Feb. 23, 1987; revision received April 25, 1988.

*Graduate Student, Aerospace Engineering. Student Member AIAA.
†Chief Scientist. Associate Fellow AIAA.
‡Professor of Mechanical and Aerospace Engineering. Associate Fellow AIAA.

Introduction

OVER the years, significant research has been directed toward the development of methods to solve the turbulent boundary-layer equations. The two general approaches for solving the set of equations are integral and finite-difference (FD) methods. Typically, the boundary-layer problem

results in a parabolic equation set for which many FD and integral methods are available.[1] Among the FD methods are variations of the Crank-Nicolson[2] and Keller box[3] schemes. Matsuno[4] has developed a noniterative, predictor-corrector method that has been applied to two- and three-dimensional laminar and turbulent flows. Integral methods require prescribed velocity profiles and empirical relations in addition to the basic conservation laws.

For any flowfield solved by a FD method, the accuracy of the results depends to a large extent on the grid resolution. The resolution requirement can cause long run times, which, in turn, increases the computational cost of the method. Knowledge of the physics of the flowfield in question allows grid points to be clustered in regions requiring high resolution. In the case of the turbulent boundary layer, grid points are clustered near the surface.

Although variable spacing, as opposed to a uniform grid, reduces the number of grid points, it is still desirable to make further reductions. The area of concentration is, again, the region near the surface which contains the majority of the grid points. An approach to this problem calls for the use of a law of the wall, which is considered to be one of the most accurate empiricisms in fluid mechanics and certainly the most accurate as far as turbulent boundary layers are concerned. Using inner variables, this law can be expressed in the most general terms as

$$u^+(y^+) = u(x,y)/u^* \tag{1}$$

where

$$y^+ = yu^*/\nu, \qquad u^* = (\tau_w/\rho)^{1/2} \tag{2}$$

This law typically applies for distances of several hundred y^+ units from the wall. The most common form is the well known log law of the wall, which is given as

$$u^+ = (1/\kappa)\,\ell n(y^+) + B \tag{3}$$

The basic concept for methods employing a law of the wall, or a wall function in two-equation models, is to describe analytically the flow from the wall to a designated point above the surface. This approach eliminates some of the highly clustered grid points near the surface, but care must be taken to ensure that the designated point is in the valid range of the law of the wall. Examples of methods implementing this approach are given by Viegas and Rubesin,[5] van Dalsem and Steger,[6] and Baldwin and Lomax.[7] The common characteristic, independent of the turbulence model, is the application of the law of the wall from the wall out to a predesignated point. The chosen point must be safely in the range of the law of the wall for all streamwise locations. This approach does not take full advantage of the law of the wall, as it limits its use to only a portion of the inner region. Walker et al.,[8] however, have developed a method that uses analytic functions in the inner region and report a reduction of approximately half the mesh points across the two-dimensional boundary layer. This result is similar to that observed with the approach described here.

The purpose of the present paper is to introduce a boundary-layer method that combines an analytic inner-layer treatment with an FD outer-layer treatment. This combination exploits the excellent empirical relationship provided by the law of the wall in the inner region and the Clauser[9] eddy viscosity in the outer region. The grid-reducing effect is maximized by applying the law of the wall out to the match point between the inner and outer regions. This match point is determined internally at each step during the computation. The FD method is used in the outer region only and can be resolved with a relatively coarse grid. Test cases are limited to two-dimensional, incompressible flows and are compared to a baseline method that applied the FD method across the entire boundary layer.

It should be noted that this new approach is extendable to compressible and three-dimensional flows. Three-dimensional laws of the wall have been developed by Johnston,[10] Mueller,[11] and others. The approach will also be valuable for use with fully viscous solutions rather than just with inviscid/boundary-layer solutions as investigated here.

Turbulence Model

A simple algebraic turbulence model of the Cebeci-Smith[3] type is used in the present investigation. In this approach, the eddy viscosity is represented by separate expressions in the inner and outer regions. The definition of the match point between the inner and outer regions results from the constraint of continuous shear stress across the entire boundary layer. This defined the match point as the point at which

$$\tau_i = \tau_o \tag{4}$$

where

$$\tau = b\rho\nu\frac{\partial u}{\partial y}, \qquad b = 1 + \frac{\nu_T}{\nu} \tag{5}$$

The eddy viscosity ν_T is given by

$$(\nu_T)_i = (\kappa y)^2\left[1 - \exp\left(-\frac{y}{A}\right)\right]^2\left|\frac{\partial u}{\partial y}\right|$$

$$A = 26\nu\sqrt{\rho/\tau_w} = 26\nu/u^*$$

$$(\nu_T)_o = K\delta^* U_e \tag{6}$$

The present approach replaces the more complex inner-layer eddy viscosity model with the law of the wall but retains the use of the outer eddy viscosity model.

Governing Equations

The Reynolds-averaged, mean velocity equations of motion for steady, two-dimensional, incompressible, turbulent boundary layers using a stream function formulation[3] are written as

$$F = f' = u/U_e \tag{7}$$

$$(F'b)' + \frac{(1+\beta)fF'}{2} + \beta(1-F^2) = x\left(F\frac{\partial F}{\partial x} - F'\frac{\partial f}{\partial x}\right) \tag{8}$$

where primes denote partial differentiation with respect to η. The similarity parameter η is normal to the surface, and β is a function of the surface coordinate x. These parameters are defined as

$$\eta = \frac{y}{x}Re_x^{1/2}, \qquad \beta = \frac{x}{U_e}\frac{dU_e}{dx} \tag{9}$$

Initial conditions for the preceding equations are obtained from the solution of the laminar boundary-layer equations at the leading edge ($x = 0$). The traditional boundary conditions are given as follows:

$$\text{no slip at the wall: } \eta = 0, \qquad F = f = 0 \tag{10}$$

$$u = U_e \text{ at } \eta = \infty, \qquad F = 1 \tag{11}$$

Since the new approach uses the FD solution from the match point to the edge, the boundary condition at the match point is

$$\text{Match point: } \eta = \eta_m, \qquad F = F_m, \qquad f = f_m \tag{12}$$

The law of the wall as given by Eq. (3) determines the values of F_m and f_m at the match point.

Finite-Difference Method

The governing equations are approximated using the two-dimensional incompressible form of Matsuno's[4] FD method. Matsuno presented a second-order-accurate, half-implicit method suitable for solving the three-dimensional laminar and turbulent boundary-layer equations; it is noniterative based on a predictor-corrector linearization. Although many methods have been demonstrated to be efficient in two dimensions, this one was chosen primarily for the benefits of using it for future three-dimensional flow applications.

The finite-difference operators used in the present investigation can be found in Ref. 12. The difference forms of the governing equations (7) and (8) are linear and can be written in a coupled, tridiagonal form for both the predictor and corrector steps as follows:

$$f_j = f_{j-1} - c_j(F_j + F_{j-1}) \tag{13a}$$

$$-A_jF_{j-1} + B_jF_j - C_jF_{j+1} + a_jf_j = D_j \tag{13b}$$

This system of equations can be solved efficiently using the Davis modified tridiagonal solver given by Blottner[13] and described here in the Appendix. Grids are generated using Blottner's[12,14] algebraic, variable spacing technique.

Inner-Outer Layer Matching

The cornerstone of the present method is the determination of the match point that separates the inner and outer regions of the turbulent boundary layer. The match point is determined from the constraint given in Eq. (4), where the inner shear stress is modeled as

$$\tau_i = \tau_w = \rho u^{*2} \tag{14}$$

based on the constant inner-layer shear stress assumption. The outer shear stress is represented by Eq. (5). The unknowns are the match point itself and the friction velocity u^*, which is part of the solution rather than a prescribed quantity.

The approach presented here uses the log law form given in Eq. (3), where κ and B are taken to the 0.41 and 5.0, respectively. When the constant inner-layer shear stress assumption and Eq. (5) for the outer layer are applied, Eq. (4) reduces to

$$\frac{u^{*2}}{\nu} = b_o \left.\frac{\partial u}{\partial y}\right|_m \tag{15}$$

Substitute the log law [Eq. (3)] into Eq. (15) to obtain

$$y_m^+ = b_o/\kappa \tag{16}$$

which determines y^+ at the match point. Using Eq. (16) for y_m^+, u_m^+ is obtained from Eq. (3). Expressions for f, F, and F' at the match point, which is generally not a grid point, are

$$f_m = (y_m^+/Re_x^{1/2})[u_m^+ - (1/\kappa)] \tag{17}$$

$$F_m = (u^*/U_e)[(1/\kappa)\,\ell n(y_m^+) + B] \tag{18}$$

$$F_m' = (u^*/U_e)^2\,[Re_x^{1/2}/(\kappa y_m^+)] \tag{19}$$

Since y_m^+ and u_m^+ are known, f_m can be calculated from Eq. (17). However, Eqs. (18) and (19) for F_m and F_m', respectively, require u^*, which is an unknown. From the definitions of y^+ and η, the product $(u^*\eta_m)$ is given by

$$(u^*/U_e)\eta_m = y_m^+/Re_x^{1/2} \tag{20}$$

The finite-difference method used to solve the boundary-layer equations in the outer region must be used to determine u^* and η_m individually.

The following procedure determines u^* and η_m. The solution procedure begins with an inward sweep from the edge of the boundary layer ($j = J_{max}$), as in the baseline method. At each grid point j, Eq. (A2) is solved, as in the conventional method, while at the same time a value of u^*/U_e is predicted from Eq. (20), assuming that this point is the match point, i.e., $\eta_m = \eta_j$. Using the predicted friction velocity, values for F_m and F_m' are determined from Eqs. (18) and (19). Then, using F_m and Eq. (A5), F_{m+1} and F_{m-1} are calculated by

$$F_{m+1} = E_{m+1}F_m + G_{m+1}f_m + e_{m+1} \tag{21}$$

$$F_{m-1} = \frac{F_m(1 - G_mc_m) - G_mf_m - e_m}{(E_m + G_mc_m)} \tag{22}$$

A three-point, central difference quotient given by

$$F_{m,n}' = \frac{(F_{m+1} - F_m) + (\Delta\eta_j/\Delta\eta_{j-1})^2(F_m - F_{m-1})}{(\Delta\eta_j/\Delta\eta_{j-1})(\Delta\eta_j + \Delta\eta_{j-1})} \tag{23}$$

is used to calculate a numerical value of F_m'. If this grid point is above the match point, then the value of $F_{m,n}'$ from Eq. (23) is greater than that from Eq. (19), and the assumption that $j = m$ is incorrect. The inward sweep is continued until $F_{m,n}'$ is less than or equal to the law of the wall F_m' given by Eq. (19). When this occurs, the match point η_m is known to lie between η_j and η_{j+1}. A typical solution is depicted in Fig. 1. The numerical solution is not continued inside of the first point below η_m. The inner part of the boundary layer is determined from the analytical solution given by Eq. (3).

It is necessary to locate the match point between grid points in order to determine an accurate value of the friction velocity. Therefore, an interpolation procedure is needed to calculate the match point. Equation (A5) can be written as

$$F_{j+1} = E_{j+1}F_j + G_{j+1} + e_{j+1} \tag{24}$$

and a Taylor series expansion about η_m is used where

$$F_{j+1} = F_m + F_m'(\eta_{j+1} - \eta_m) \tag{25a}$$

$$F_j = F_m - F_m'(\eta_m - \eta_j) \tag{25b}$$

$$f_j = f_m - F_m(\eta_m - \eta_j) + F_m'(\eta_m - \eta_j)^2/2 \tag{25c}$$

Substitution of the known value of f_m from Eq. (17) and F_m and F_m' from Eqs. (18) and (19) into Eq. (25) and then the

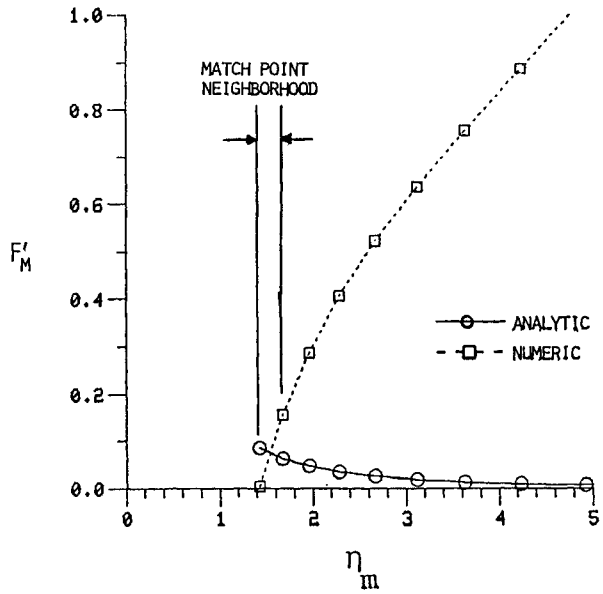

Fig. 1 Match point location procedure.

result into Eq. (24) yields a single equation of the form

$$C_1(u^*/U_e)^2 + C_2(u^*/U_e) + C_3 = 0 \tag{26}$$

The coefficients for this equation are known and given by

$$C_1 = (\eta_{j+1} - E_{j+1}\eta_j - G_{j+1}\eta_j^2/2)Re_x^{1/2}/(\kappa y_m^+) \tag{27a}$$

$$C_2 = (u_m^+ - 1/\kappa)(1 - E_{j+1} - G_{j+1}\eta_j) \tag{27b}$$

$$C_3 = G_{j+1}y_m^+/(2\kappa Re_x^{1/2}) - e_{j+1} \tag{27c}$$

The resulting value of u^*/U_e is then used to determine f and F at the first grid point below η_m such that the outer region computation can be computed with the FD method. Note that Eq. (A2) has been solved during the sweep inward in the match point location procedure, and the outward sweep of Eq. (A5) to the edge of the boundary layer completes the outer-region solution. When applying the expressions based on the law of the wall, functions of x are evaluated at $i + \frac{1}{2}$ for the predictor and $i + 1$ for the corrector.

The procedure just described was also applied using the law of the wall given by Liakopolous,[15] and the details are given in Ref. 16. This law is given by

$$u^+ = \ln\left[\frac{(y^+ + 11)^{4.02}}{(y^{+2} - 7.37y^+ + 83.3)^{0.79}}\right] + 5.63\tan^{-1}(0.12y^+ - 0.441) - 3.81 \tag{28}$$

It includes the laminar sublayer and the overlap region for moderate pressure gradients. Results are presented using the log law and the Liakopolous law, which will be referred to as laws 1 and 2, respectively.

Results and Discussion

Prior to implementing the new approach, Matsuno's[4] FD method was applied across the entire boundary layer for laminar and turbulent flows. Results using this approach, which is referred to as the baseline method, are documented in Ref. 16.

Test cases for the new approach are presented for steady, incompressible flow over flat plates and a $BA = 0.6$ ellipse, where BA is the ratio of the semiminor $\bar{b}$ to semimajor $\bar{a}$ axes of the ellipse. An angular coordinate ϕ, which is zero at $x = 0$, is defined by

$$\cos\phi = -(X - \bar{a})/\bar{a}, \qquad \sin\phi = Y/\bar{b} \tag{29}$$

Cartesian coordinate (X, Y) axes are defined with the origin at the ellipse stagnation point. The reference length L is measured along the major axis of the ellipse and $\bar{x} = x/L$. Further details on the ellipse problem can be found in Refs. 12 and 16.

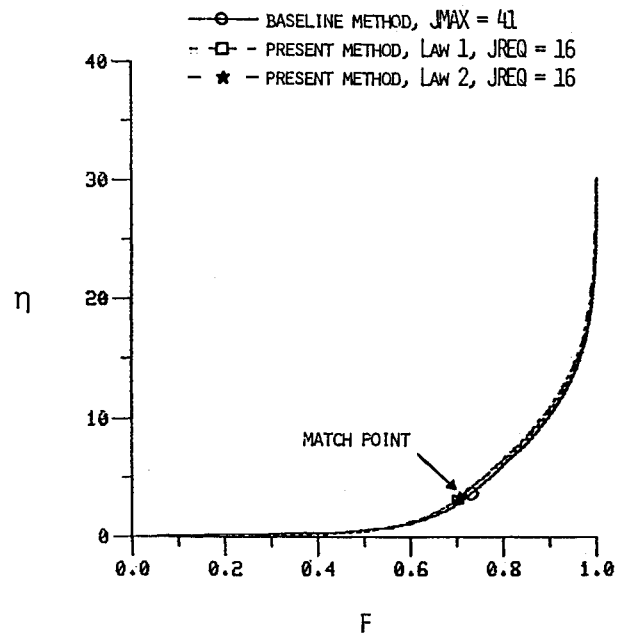

Fig. 2a Flat-plate velocity profile at $\bar{x} = 1.0$, $Re = 1 \times 10^6$.

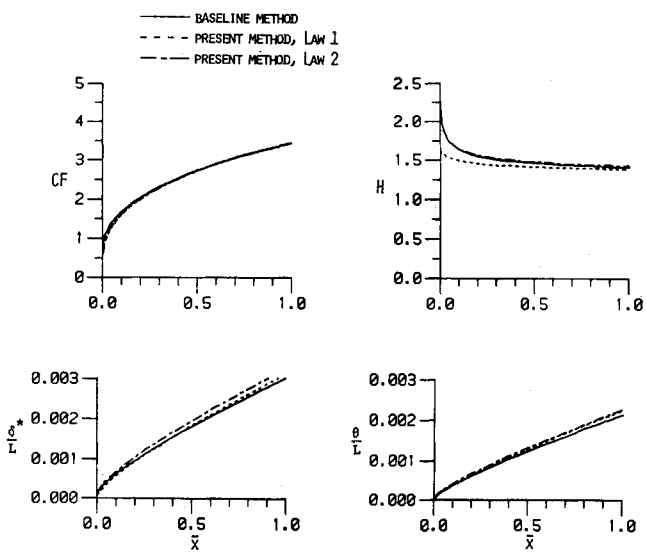

Fig. 2b Flat-plate flow parameters for $Re = 1 \times 10^6$, $J_{max} = 41$.

Table 1 Flat-plate results for the baseline and present methods at $\bar{x} = 1$

Method	J_{max}	Range of J_{req}[a]	J_{req}	CF, % error	H, % error	δ^*, % error	θ, % error
Baseline	241[b]	241	241	0.0	0.0	0.0	0.0
Baseline	41	41	41	0.261	0.107	0.197	0.089
Baseline	26	26	26	0.382	0.291	0.490	0.197
Baseline	16	16	16	−0.680	0.704	2.190	1.473
Baseline	11	11	11	7.272	6.163	−15.768	−20.658
Present, law 1	41	16–23	16	0.926	−1.727	3.627	5.445
Present, law 1	26	11–15	11	1.014	−1.670	3.597	5.356
Present, law 1	16	7–9	7	0.848	−1.550	4.627	6.275
Present, law 2	41	16–19	16	0.579	0.583	7.817	7.194
Present, law 2	16	7–8	7	0.596	0.697	8.648	7.893

[a]For the range of $0 \le \bar{x} \le 1$. [b]Exact values: $CF = 3.4099385$, $H = 1.4068$, $\delta^* = 0.0029997$, $\theta = 0.0021323$.

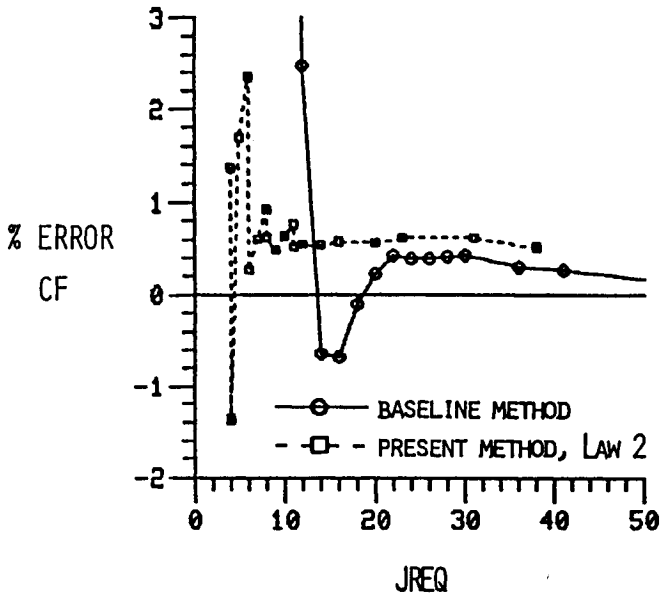

Fig. 3a Effect of J_{req} on percent error in CF for a flat plate at $\bar{x} = 1.0$, $Re = 1 \times 10^6$.

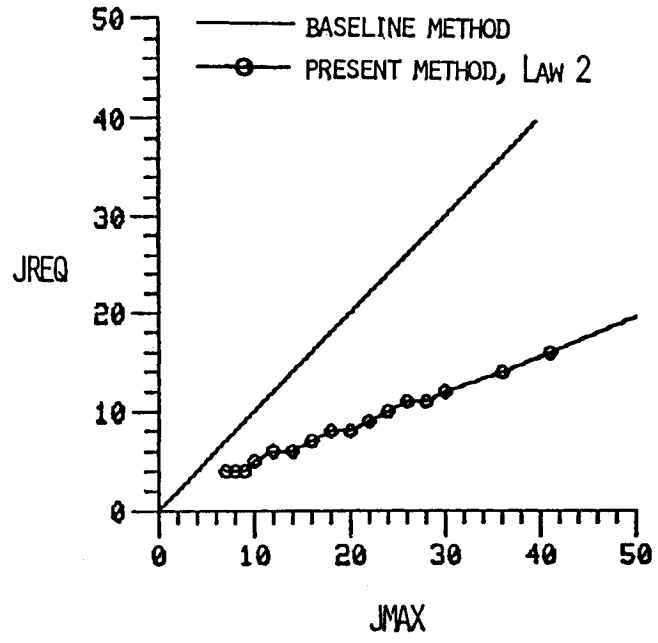

Fig. 3b Grid points required for a flat plate at $\bar{x} = 1.0$, $Re = 1 \times 10^6$.

Grids are designated by the number of points J_{req} across the boundary layer which are required for the finite-difference part of the solution. For the baseline method, the number of grid points across the entire boundary layer is called J_{max}, which is also J_{req}. However, since the present method uses Eq. (3) or (28) for the inner region, J_{req} is the number of grid points used in the outer-region finite-difference solution.

Laws 1 and 2, given by Eqs. (3) and (28), respectively, were used to model the inner region for flow over a flat plate. Test cases for law 1 include grids with $J_{max} = 41$, 26, and 16 points across the entire boundary layer for the baseline solution. The important parameter for the present method is, however, the number of grid points actually used for the outer region J_{req} rather than the total number J_{max}. The J_{req} parameter varies in the streamwise direction due to the shift in the match point as the boundary layer grows. For the $J_{max} = 41$ grid, J_{req} varies between 16 and 23 points. For the $J_{max} = 26$ grid, J_{req} varies between 11 and 15 points, whereas J_{req} varies between 7 and 9 points for the $J_{max} = 16$ grid. The largest values of J_{req} occur near the leading edge, where the boundary layer is primarily laminar. Law 2 test cases were calculated with $J_{max} = 41$ and 16. J_{req} varied between 16 and 19 for $J_{max} = 41$ and between 7 and 8 for $J_{max} = 16$. The difference in J_{req} for laws 1 and 2 near the leading edge is because law 2 includes the laminar sublayer, whereas law 1 does not. For comparison purposes, the exact solution was taken to be the result generated by the baseline method with a 31×241 ($\Delta x \times \Delta\eta$) grid. In addition to velocity profiles, comparisons are made for a skin-friction parameter ($CF = C_f Re_x^{1/2}$), nondimensional displacement and momentum thicknesses (δ^*/L and θ/L), and the shape factor ($H = \delta^*/\theta$).

Figure 2a shows the flat-plate velocity profile at $\bar{x} = 1$ ($Re_x = 1 \times 10^6$) computed with the baseline method and the present method using laws 1 and 2 for the inner region. The profiles show good agreement but, in general, show a slightly smaller velocity for the present solutions as compared to the baseline solution. The exception is the region near the wall as computed using law 1, where the lack of a sublayer treatment causes a small velocity increase as compared to the baseline and law 2 solutions. The flow parameters CF, δ^*, θ, and H for this case are given in Fig. 2b. Table 1 shows the percent error for these flow parameters at the $\bar{x} = 1$ station. The $J_{max} = 16$ grid case for laws 1 and 2 and the $J_{max} = 26$ grid case for law 1 are also given in Table 1. Note that the present method using law 2 computes CF with a 0.596% error using only seven points in the outer region ($J_{max} = 16$). Flow parameter distributions for this case are nearly identical to those shown in Fig. 2b. Since the calculation of δ^*, θ, and H relies on the integration of the velocity profile, laws 1 and 2 are not expected to give the same result, since law 1 does not include the laminar sublayer. Neither law 1 nor law 2 should be expected to duplicate the baseline result, due to the differing inner-layer treatments.

Figure 3a shows the error in CF as a function of J_{req} at $\bar{x} = 1$. Less than 1% error in CF is obtained for J_{req} greater than 6 for the present method, whereas the baseline method requires $J_{req} = J_{max}$ greater than 13 for comparable accuracy. Figure 3b shows the grid reduction of approximately 60% for the present method relative to the baseline method at $\bar{x} = 1$ on the flat plate.

A comparison was made with the experimental Weighardt flat-plate flow used in the 1968 Stanford Conference[17] and designated as flow 1400. This experiment was conducted at $Re = 1.09 \times 10^7$. Figure 4a shows the velocity profiles from the baseline method and the law 1 form of the present method at $\bar{x} = 1$, which corresponds to the last station given in Ref. 17. The $J_{max} = 41$ grid was used, which resulted in $J_{req} = 15$ for the present method at $\bar{x} = 1$. Skin-friction and shape factor distributions for this case are given in Fig. 4b. Both computational methods provide good predictions of the experimental results. It is clear, however, that the present method computes the zero pressure gradient case with a significant reduction in the number of grid points.

The effect of pressure gradient was investigated for flow over ellipses. The δ^*, θ, H, and velocity distributions are predicted with an accuracy comparable to that of the flat-plate cases. The major effect of the pressure gradient on the present method is the poorer prediction of CF. Figure 5 shows the CF comparison as computed on the 91×41 grid at $Re = 1 \times 10^6$. With law 2, J_{req} varies between 14 and 23 with the present method. The trends of the two distributions are similar, but the agreement is poor. Results for other ellipses[12,16] along with this case demonstrate the need for pressure gradient effects to be incorporated into the present method.

Computations for the ellipse cases using the present method were stopped short of separation because laws 1 and 2 are not valid near separation. An example of the velocity profile using law 2 near separation is given in Fig. 6 for the $BA = 0.6$ ellipse at $\phi = 130$ deg. Separation as computed by the baseline

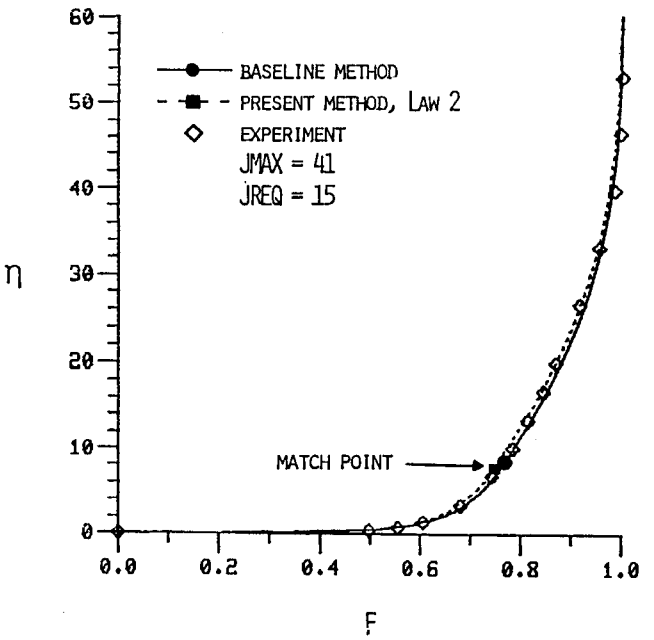

Fig. 4a Flat-plate velocity profile at $\bar{x} = 1.0$, $Re = 1.09 \times 10^7$.

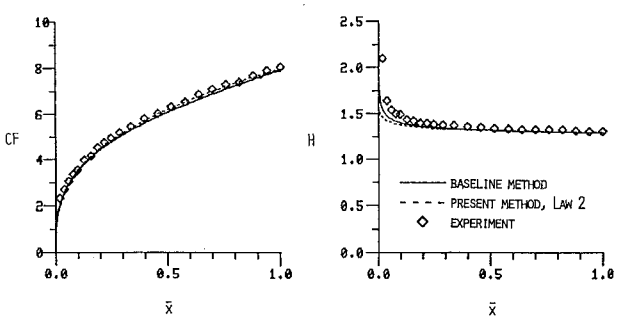

Fig. 4b *CF* and *H* distributions for a flat plate, $Re = 1.09 \times 10^7$.

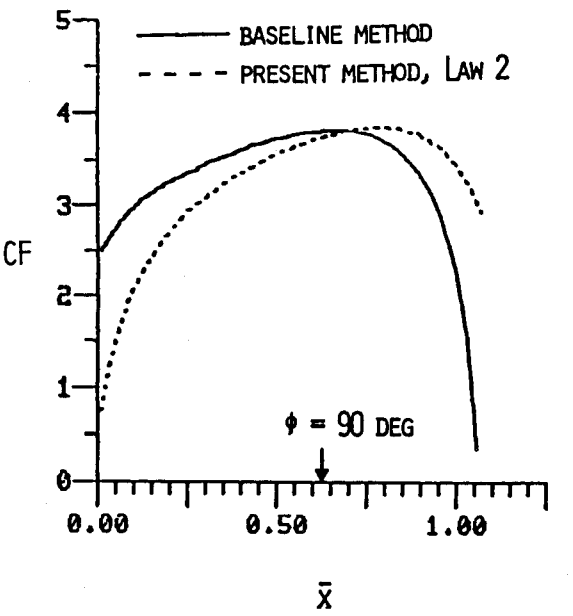

Fig. 5 *CF* distribution for the $BA = 0.6$ ellipse.

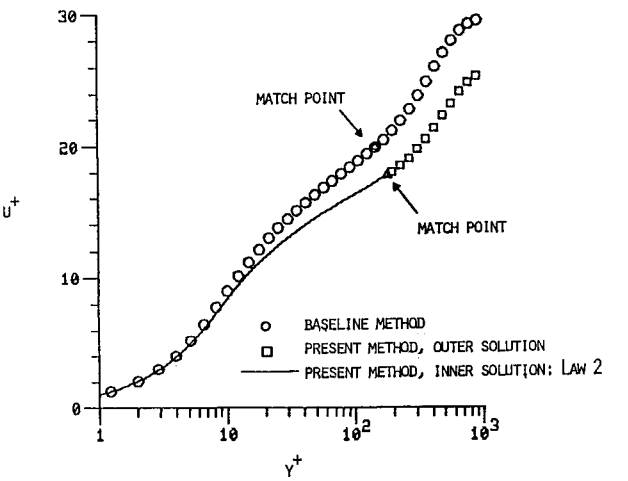

Fig. 6 Inner variable velocity profile at $\phi = 130$ deg on the $BA = 0.6$ ellipse.

method, which is defined as the point where $CF = 0$, occurs at $\phi = 143$ deg for this case. The present method is forced to match law 2 below the match point, which gives a result quite different from the baseline method. As separation is approached, law 2 moves further away from the baseline profile.

To see the pressure gradient effect more clearly, the shear stress was calculated across the boundary layer. Figure 7 shows a representative distribution ($\phi = 70$ deg) for the $BA = 0.6$ ellipse. The baseline and present method (law 2) results are referenced to τ_w and η_e of the baseline method. The symbols mark the η/η_e position of the match points. Note that the assumed constant inner-region shear stress shown for the present method does not compare with the variation computed by the baseline method. The momentum equation shows that a shear stress gradient (in the y direction) proportional to the pressure gradient exists at the wall. These results show that the constant inner-layer shear stress assumption is not adequate in the presence of strong pressure gradients. The shear stress distribution, given by the baseline method in Fig. 7, also shows an unusual characteristic. Note the sharp peak, which always occurs at either the grid point directly above or below the match point, indicating a discontinuous shear stress gradient. This is not a physical problem but a numerical problem resulting from the abrupt shift from the inner- to outer-region eddy viscosity.

A modification was introduced to partially account for pressure gradient effects. Laws 1 and 2 were modified by adding White's linear wake function,[18] which is given as

$$WF = 0.6\alpha y^+, \qquad \alpha = \frac{\nu}{\tau_w u^*}\frac{dp}{dx} = -\frac{\beta}{Re_x}\left(\frac{U_e}{u^*}\right)^3 \tag{30}$$

Law 1, given by Eq. (3), is modified as follows:

$$u^+ = (1/\kappa)\,\ell n(y^+) + B + WF \tag{31}$$

Law 2 is modified in a similar manner. Equations for $\partial u^+/\partial y^+$, f_m, F_m, and F_m' are easily modified also. The present method has been tested with this modification applied to law 1. However, values of f_m were determined from the modified form of law 2 as more accuracy is obtained due to the treatment of the laminar sublayer. Presently, inner and outer eddy viscosities as given by Eq. (6), respectively, are matched, resulting in

$$\kappa y_m^+ [1 - \exp(-y_m^+/26)]^2 = (\nu_T/\nu)_o \tag{32}$$

which requires a short iterative procedure to solve for y_m^+. The remaining part of the solution procedure is identical to that described earlier.

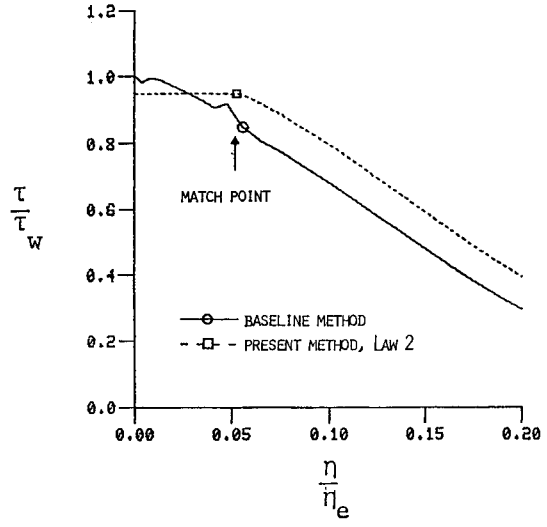

Fig. 7 Shear stress distribution at $\phi = 70$ deg on the $BA = 0.6$ ellipse.

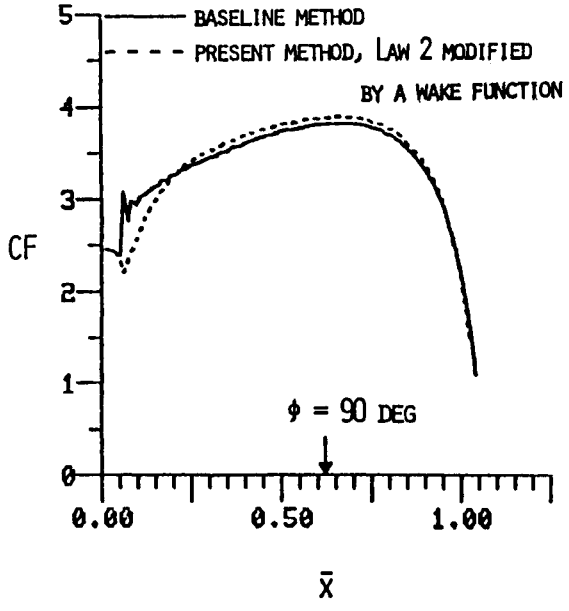

Fig. 8 *CF* distribution for the $BA = 0.6$ ellipse.

The $BA = 0.6$ ellipse was used as a test case. Solutions were computed with laminar flow existing from $\phi = 0$–10 deg. At this point, the turbulence terms were introduced without a gradual transition region. Figure 8 shows the improved *CF* prediction, as compared to Fig. 5, using $Re = 1 \times 10^6$ and the $J_{max} = 41$ grid.

Conclusions

The following conclusions are drawn from the present study:

1) A new method was developed for turbulent boundary layers which described the inner region with a law of the wall and calculates the outer region by a finite-difference method.

2) The number of grid points across the boundary layer required to calculate a solution by the finite-difference method was reduced by approximately 50% by using grid points only in the outer region with the new method.

3) The new method predicted accurate displacement and momentum thicknesses over flat plates and ellipses. The skin friction was predicted well for the flat plate, but the accuracy decreased significantly for the ellipses when the inner region was described by the law of the wall alone.

4) The assumption of constant shear stress across the inner region, which was used in the law of the wall, was found to be inadequate to calculate skin friction in the presence of pressure gradients.

5) Adding a wake function to the law of the wall allows some of the pressure gradient effect to be taken into account, thereby increasing the accuracy of the method.

Appendix: Davis Modified Tridiagonal Solver

The following procedure is used when solving the coupled, linear tridiagonal equations given by Eq. (13). First, the following parameters are determined during an inward sweep from the edge of the boundary layer (obtained from boundary conditions at the outer edge):

$$E_{J_{max}} = 0, \qquad G_{J_{max}} = 0, \qquad e_{Jmax} = 1 \tag{A1}$$

For $j = J_{max} - 1, J_{max} - 2, \ldots, 2$

$$E_j = [A_j - c_j(C_j G_{j+1} - a_j)]/DEN$$

$$G_j = (C_j G_{j+1} - a_j)/DEN$$

$$e_j = (D_j + C_j e_{j+1})/DEN \tag{A2}$$

where

$$DEN = B_j - C_j E_{j+1} + c_j(C_j G_{j+1} - a_j) \tag{A3}$$

The solution is then obtained during an outward sweep from the following:

$$F_1 = 0, \qquad f_1 = 0 \qquad \text{(wall boundary conditions)} \tag{A4}$$

$$F_j = E_j F_{j-1} + G_j f_{j-1} + e_j$$

$$f_j = f_{j-1} - c_j(F_j + F_{j-1}) \qquad j = 2,3,\ldots,J_{max} \tag{A5}$$

Equation (A4) is the standard, no-slip boundary condition at the wall which is replaced by the match point conditions in the present method.

Acknowledgment

This investigation was supported by the Graduate Researchers Program Grant NGT 34-003-803 through NASA Headquarters and the High Reynolds Number Aerodynamics Branch of the Transonic Aerodynamics Division at NASA Langley Research Center.

References

[1]Anderson, D. A., Tannehill, J. C., and Pletcher, R. H., *Computational Fluid Mechanics and Heat Transfer,* McGraw-Hill, New York, 1984.

[2]Blottner, F. G., "Computational Techniques for Boundary Layers," AGARD Lecture Series No. 73, 1975.

[3]Cebeci, T. and Smith, A. M. O., *Analysis of Turbulent Boundary Layers,* Academic Press, New York, 1974.

[4]Matsuno, K., "A Vector-Oriented Finite Difference Scheme for Calculating Three-Dimensional Compressible Laminar and Turbulent Boundary Layers on Practical Wing Configurations," AIAA Paper 81-1020, June 1981.

[5]Viegas, J. R. and Rubesin, M. W., "Wall-Function Boundary Conditions in the Solution of the Navier-Stokes Equations for Complex Compressible Flows," AIAA Paper 83-1694, July 1983.

[6]Van Dalsem, W. R. and Steger, J. L., "The Efficient Simulation of Separated Three-Dimensional Viscous Flows Using the Boundary Layer Equations," AIAA Paper 85-4064, Oct. 1985.

[7]Baldwin, B. S. and Lomax, H., "Thin Layer Approximation and Algebraic Model for Separated Turbulent Flows," AIAA Paper 78-0257, Jan. 1978.

[8]Walker, J. D. A., Ece, M. C., and Werle, M. J., "An Embedded Function Approach for Turbulent Flow Prediction," AIAA Paper 87-1464, June 1987.

[9]Clauser, F. H., "The Turbulent Boundary Layer," *Advances in Applied Mechanics,* Vol. 4, 1956, pp. 2-51.

[10]Johnston, J. P., "On the Three-Dimensional Turbulent Boundary-Layer Generated by Secondary Flow," *Journal of Basic Engineering,* Vol. 82, No. 1, March 1960, pp. 233-248.

[11]Mueller, U. R., "Measurement of the Reynolds Stresses and the Mean Flow Field in a Three-Dimensional Pressure-Driven Boundary Layer," *Journal of Fluid Mechanics,* Vol. 119, June 1982, pp. 121-153.

[12]Wahls, R. A., Barnwell, R. W., and DeJarnette, F. R., "A Finite-Difference Outer Layer and Integral Inner Layer Method for the Solution of the Turbulent Boundary Layer Equations," AIAA Paper 87-429, Jan. 1987.

[13]Blottner, F. G., "Computational Techniques for Boundary Layers," Sandia Lab., Albuquerque, NM, Rept. SAND-79-0893, 1979.

[14]Blottner, F. G., "Nonuniform Grid Method for Turbulent Boundary Layers," *Lecture Notes in Physics,* Vol. 35, 1975, pp. 91-97.

[15]Liakopolous, A., "Explicit Representations of the Complete Velocity Profile in a Turbulent Boundary Layer," *AIAA Journal,* Vol. 22, June 1984, pp. 844-846.

[16]Wahls, R. A., "Solution of the Turbulent Boundary-Layer Equations by a Finite-Difference Outer Layer and Integral Inner Layer Method," M.S. Thesis, North Carolina State Univ., Raleigh, NC, June 1986.

[17]Coles, D. and Hirst, E. A., (eds.), *Computation of Turbulent Boundary Layers—1968 AFOSR-IFP-Stanford Conference,* Vol. 2, Stanford Univ. Press, Stanford, CA, 1968.

[18]White, F. M., *Viscous Fluid Flow,* McGraw-Hill, New York, 1974, p. 523.